Available online at www.CivileJournal.org

Civil Engineering Journal

(E-ISSN: 2476-3055; ISSN: 2676-6957)

Vol. 11, No. 12, December, 2025

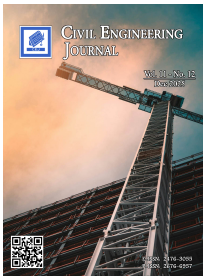

Combined Effect of Basalt Fibers and Bentonite Clay on Complex Mortar Properties

Hasmik Karamyan [1], Mariam Avagyan [1], Roza Shainova [1*], Anush Sahakyan [1], Armine Baghdagyulyan [1], Gevorg Tepanosyan [2], Zhenya Poghosyan [2], Araksya Aperyan [3], Yeghvard Melikyan [4], Maria Badalyan [1]

[1] *Faculty of Construction, National University of Architecture and Construction of Armenia, Yerevan 0009, Armenia.*

[2] *The Center for Ecological-Noosphere Studies, NAS, Yerevan 0025, Abovyan-68, Armenia.*

[3] *Institute of Geological Sciences of the National Academy of Sciences of Armenia, Yerevan, 0019, Armenia.*

[4] *Innovation Center for Nanoscience and Technologies, A.B. Nalbandyan Institute of Chemical Physics NAS RA, Yerevan 0014, Armenia.*

Received 27 August 2025; Revised 19 October 2025; Accepted 25 November 2025; Published 01 December 2025

Abstract

This study examined the effects of basalt microfibers and amorphous-structured bentonite clay on the properties of complex mortar mixtures composed of cement and quicklime, utilizing locally sourced raw materials. Bentonite clay was subjected to thermal treatments at 400, 600, and 1000°C, and a technogenic pozzolanic additive was incorporated to investigate its influence on mortar performance. Optimal results were observed for the clay treated at 600°C, which was subsequently used in the mortar formulations. The primary objective was to assess the effects of varying basalt microfiber dosages (0.5%, 1%, and 2%) and thermally treated bentonite clay concentrations (5%, 15%, and 25%) on the chemical composition, physico-mechanical properties, and structural development of the resulting multi-component systems. Advanced analytical techniques, including SEM/EDS, XRD, FTIR, XRF, DLS, and thermochemical analyses (TG/DTG, TG/DSC, and TG/MS), were used to evaluate the mineralogical composition, particle size distribution, microstructure, and thermal behavior. The findings show that the combined use of basalt microfibers and thermally treated bentonite clay significantly enhanced the mechanical strength and structural formation of the mortars. This study provides novel insights into the synergistic effects of these components, offering a promising approach for enhancing mortar performance using locally sourced materials.

Keywords: Basalt Microfiber; Complex Mortar Mix; Microfiller; Montmorillonite; Pozzolanic Activity; Thermal Behavior.

1. Introduction

According to global CO_2 emissions statistics, the construction sector ranks as the third-largest polluting industry, exerting a substantial impact on global warming processes [1, 2]. This issue primarily arises from the extensive production of Portland cement-based concrete [3]. International estimates indicate that the production of Portland cement accounts for approximately 8–9% of global CO_2 emissions [4–9]. Furthermore, the production of each ton of clinker results in an average emission of 0.8–0.9 tons of carbon dioxide [10–12], with approximately 50% of these emissions occurring during the calcination phase due to the decarbonation of calcium carbonate (approximately 0.53 tons), while the remainder originates from fuel combustion and energy consumption [13, 14]. Given the urgency of

* Corresponding author: rozashainova@nuaca.am

http://dx.doi.org/10.28991/CEJ-2025-011-12-05

mitigating these environmental impacts, numerous researchers have emphasized the role of sustainable materials and low-carbon cement alternatives in reducing emissions across the construction industry [15, 16].

The imperative to reduce emissions necessitates the development of complex mortar mixes utilizing innovative technologies. In this context, natural and artificial pozzolanic active additives assume significant importance, as they facilitate the partial replacement of Portland cement, thereby not only reducing emissions, depending on the type and quantity of the substitute used [17], but also significantly enhancing the technical performance of the mortars [18–20]. Evidence of the effective utilization of pozzolanic additives can be traced back to ancient Roman structures, where lime-based mortars achieved notable strength, water resistance, and durability due to the incorporation of pozzolanic materials [21-23]. This historical practice is further corroborated by contemporary scientific research, which underscores the significance of these additives not only for the partial substitution of Portland cement but also for enhancing the mechanical and functional properties of mortars and concrete mixes employed in restoration and reinforcement projects [24-27]. However, despite extensive studies on traditional pozzolans, there is limited information on the performance of locally sourced bentonite clays subjected to controlled thermal treatment as pozzolanic additives, especially in combination with fibers and quicklime.

In parallel, fibrous materials have been increasingly incorporated into mortar compositions to enhance tensile and flexural strength, control shrinkage, and improve crack resistance. Although traditional organic fibers have been historically used, contemporary research has focused on advanced fibers such as carbon, glass, polypropylene, and basalt [28–30]. Among these, basalt fibers stand out because of their excellent mechanical performance, chemical and thermal stability, resistance to corrosion, and environmental friendliness. Several studies have demonstrated that the inclusion of basalt fiber improves the crack bridging capacity, flexural behavior, and post-cracking toughness of cementitious composites [31–38]. Nevertheless, most studies have examined basalt fibers in relatively simple mortar or concrete systems, and systematic investigations combining basalt fibers with pozzolanic additives and quicklime in complex multi-component mortars are lacking.

Although many investigations have focused on the individual effects of basalt fibers or pozzolanic additives, few have explored their combined impact, particularly in systems containing quicklime and thermally treated bentonite clay. Thermally activating bentonite or montmorillonite clays at moderate temperatures (400–800 °C) increases their reactivity by altering their structure, enabling their use as effective pozzolanic materials [39, 40]. However, there is limited research on the synergistic behavior of basalt microfibers and thermally treated bentonite clay in quicklime-cement mortars, which is a notable gap in sustainable materials science.

Recent studies have begun to investigate how pozzolanic additives and fibers interact in mortar systems, revealing that their combination can significantly improve the mechanical properties and microstructural performance [41, 42]. However, the combined use of basalt microfibers, thermally treated bentonite, and quicklime in complex mortar systems remains poorly understood, especially when sourced from local raw materials.

The novelty of this study lies in its systematic investigation of the combined effects of basalt microfibers, thermally treated bentonite clay (montmorillonite), and quicklime in multi-component mortar systems. This was achieved through the application of a technogenic pozzolanic additive subjected to thermal treatment at varying temperature regimes: 400, 600, and 1000°C [43], and the task was to determine if thermally treated additives could be classified as Class N pozzolans in accordance with the provisions of the ASTM C618 standard [44].

In this study, we examined the physico-mechanical properties of complex mortar mixes developed using locally sourced raw materials, with varying contents of basalt microfibers (0.5%, 1%, and 2%) and thermally treated amorphous-structured bentonite clay/montmorillonite (5%, 15%, and 25%) at 600 °C. This approach directly addresses the identified gaps in the literature by combining fiber reinforcement with thermally activated pozzolanic additives in complex, locally sourced mortar systems, allowing for the evaluation of both mechanical performance and compliance with international standards.

2. Materials and Methods

The research entailed a thorough examination of enhanced mortar mixtures and their constituents through the application of advanced microstructural, chemical, and physicochemical analytical techniques. Specifically, analyses were conducted using scanning electron microscopy (SEM JEOL JCM-7000), X-ray fluorescence spectroscopy (Rigaku NEX DE XRF), and X-ray diffraction (XRD), complemented by particle size distribution evaluation via dynamic light scattering (DLS, Litesizer 500 by Anton Paar). Furthermore, infrared spectroscopy (Shimadzu, IR Tracer 100) was utilized to characterize structural transformations and assess pozzolanic activity.

The porous structure and surface properties were analyzed using the Brunauer-Emmett-Teller (BET, Micromeritics ASAP 2020 Plus 2.00) method at a liquid nitrogen temperature of 77K. This analysis was based on the variation in nitrogen adsorption quantities resulting from gradual changes in relative pressure (P/P_0). X-ray diffraction (XRD) analysis was conducted using the Rigaku MimiFlex instrument with copper (CuKα) radiation, which has a wavelength

of approximately 1.5406 Å, scanning within the 3–145° (2θ) range. As primary binders in the complex mortar mix, Portland cement 500M, produced by the Ararat Cement Plant and 96% active air quicklime produced in Vedi "GOLD LIME" LLC were utilized. To enhance the structural integrity of the mix and mitigate shrinkage-related adverse effects, basalt microfibers with a diameter of 17 μm and a length of 6 mm were incorporated. Their inclusion contributed to the improvement of the mechanical strength of the complex mortar by reducing the likelihood of crack formation and enhancing the overall structural resistance.

2.1. Raw Materials

The M500 (52.5N class, Ararat Cement Corporation LLC) cement plant was used as the binding material in the processed compositions. Table 1 presents the mechanical and physical characteristics of Portland cement and its chemical composition [45-47] as available from the commercial datasheet.

Table 1. Physical properties and chemical composition of cement

Characteristics								
Standard consistency (%)					30			
Specific gravity (g/sm^3)					3.1			
Blain's fineness (m^2/kg)					328.3			
Compressive strength (MPa)					23		3 days	
					38		7 days	
					51.5		28 days	
Setting time (min)					55		Initial	
					285		Final	
Chemical composition of cement (wt. %)								
SiO_2	Al_2O_3	Fe_2O_3	MgO	CaO	SO_3	Loss on ignition	Insol. Resid.	Free CaO
22.1	4.3	1.2	1.1	62.9	2.1	3.2	1.9	1.1

The average particle size of the sand is shown in Table 2.

Table 2. Grain size composition of basalt sand

Name of rocks	Whole residues on the sieves (g)		
	0.63	0.315	0.16
Basalt sand	673	535.4	278.8

In the present study, basalt fiber produced by the "ArmBasalt" Continuous Basalt Fiber Manufacturing Plant CJSC was selected as the dispersed reinforcing material, and the composition of the oxides is presented in Table 3. The use of this fibre contributes not only to the enhancement of the mechanical performance of the composite but also to its durability under various environmental and thermal conditions.

Table 3. Quantitative indicators of the main oxides in thermally treated clay and basalt microfibers by XRF

Materials	Quantitative composition of oxides (%)											
	SiO_2	Al_2O_3	TiO_2	Fe_2O_3	FeO	CaO	MgO	P_2O_5	MnO	Na_2O	K_2O	H_2O
Calcined clay	59.01	19.11	0.37	3.07	3.04	5.04	6.02	0.12	0.02	1.11	1.63	0.25
Basalt fiber	34.35	31.53	0.43	2.95	-	2.68	-	-	-	-	-	-

Furthermore, the X-ray fluorescence (XRF) analysis of the montmorillonite additive, after thermal treatment at 600°C for two hours, revealed that the material developed a predominantly amorphous structure (Figure 1). According to the chemical composition results, this thermally activated clay met the requirements for Class N pozzolanic materials, as defined by ASTM C618 [44]. The analysis indicated a high concentration of reactive oxides SiO_2, Al_2O_3, and Fe_2O_3, the combined content of which exceeded the minimum threshold specified by the standard, confirming the significant pozzolanic activity of the material (Table 3).

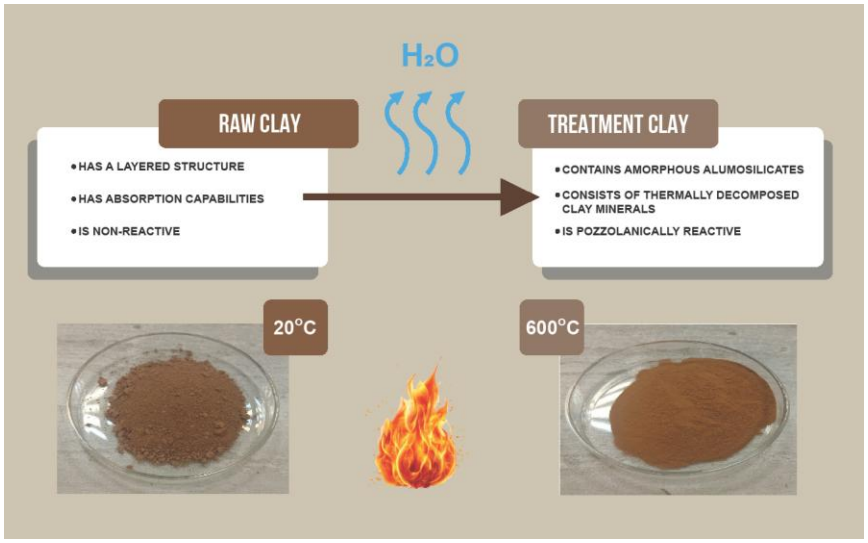

Figure 1. Thermal Treatment of Clay

- ***Compositions and Specimen Preparation***

To ensure a fair comparison between mortars with and without basalt fibers. The basalt fiber dosages were chosen according to the amount of content in 1 m^3 of the mortar, with a measurement unit of kg/m^3. Laboratory research was conducted using three identical test samples of size 40 × 40 × 160 mm. Different mortars, including the Control and Control+montmorillonite (CM) mixtures, were developed, as presented in Table 4.

Table 4. Quantities of starting materials for components

N	Basalt | Sand (g)	Treatment clay 15% (g)	Quicklime (g)	Gypsum (g)	Cement (g)	Water (ml)	Basalt fiber (%)	Water-repellent (g)
Control	1439	-	80	4	300	327	-	11.2
CM	1439	45	80	4	300	327	-	11.2
CM	1439	45	80	4	300	327	0.5	11.2
CM	1439	45	80	4	300	327	1	11.2
CM	1439	45	80	4	300	327	2	11.2

The components were mixed in dry form using a mortar mixer (Mortar mixer, Matest), after which the basalt fiber was added, and the mixing process was continued. The required amount of mixing water, together with the bulk water-repellent (IDROCRETE DM, MAPEI), was then introduced, and mixing was continued until a homogeneous mass was obtained. The completed mixture was subsequently transferred into the metal molds. Consequently, six test specimens for each composition were prepared in prism shapes with dimensions of 40×40×160 mm. After 24 h, the specimens were removed from the molds and placed in a storage chamber set to a temperature of (20±2) °C and (91-95) % relative humidity for 28 days. The flexural and compressive strengths of the specimens were assessed at 7 and 28 days, along with their humidity absorption at 28 days, as listed in Section 2.2. The processes involved in the production of mortars are illustrated in Figure 2: combining the raw components, preparing the cement mortar, casting the test specimens, curing them under humid conditions, and subjecting them to flexural and compressive strength testing [46].

Figure 2. Preparation of mortar mixtures and test specimens

2.2. Physical and Mechanical Characterization of Mortars

2.2.1. Water Absorption Measurement

After 28 days the water absorption of cement mortars was determined according to the EN 196-1-2002 [46] standard. To determine the water absorption, for the laboratory tests we used Italian "Matest" manufacturer equipment, such as measuring calipers with 0.01 mm accuracy and a V073-01 balance with 0.1 g accuracy.

The flexural and compressive tests were carried out at two time points, namely after curing of 7 and 28 days.

2.2.2 Flexural Strength

The flexural strength of the specimens was tested using testing equipment, specimen size of 40 × 40 × 160 mm. A three-point flexural test on a poured prism formed the basis of the experiment using standard EN 196-1-2002 [46].

2.2.3. Compressive Strength

In accordance the compressive strength was determined by the average value of six test specimens, using standard EN 196-1-2002 [46], and the specimen size was 40 mm × 40 mm. Compressive tests were performed on an automatic pressure machine.

3. Results and Discussion

3.1. FTIR, XRD and DLS Analysis

The pozzolanic behavior is influenced not only by the oxide composition but also by various morphological and structural factors, including the presence of an amorphous phase, a high specific surface area, and the particle size distribution and dispersion characteristics of the fine material. These attributes are verified through analyses such as FTIR, XRD, and DLS (Figure 3).

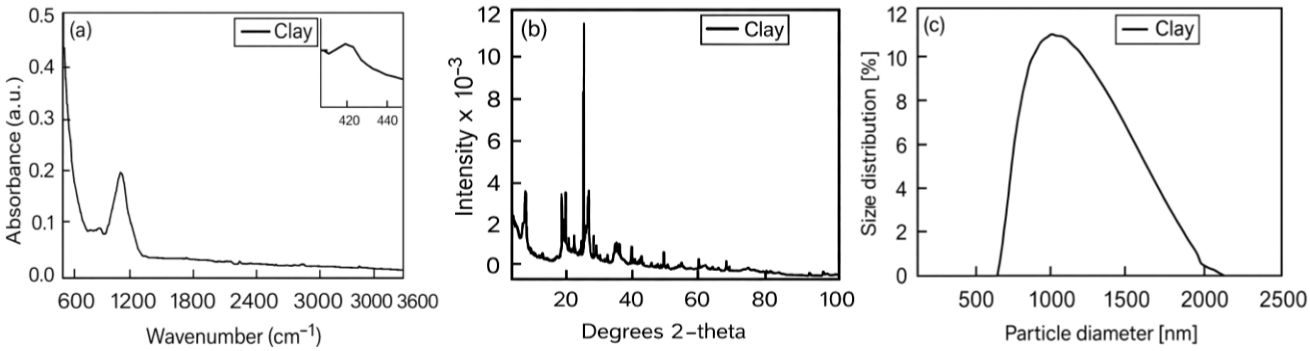

Figure 3. Combined analysis of the montmorillonite additive by (a) spectroscopic, (b) crystallographic, and (c) particle size distribution methods

The FTIR results indicated that the thermally treated sample retained its primary structural features, which suggests the partial stability of aluminosilicate units (Si–O–Si and Al–O–Si) and the reorganization of metal-oxide bonds (Al/Fe). The FTIR results (Table 5) highlight the key structural features indicative of high pozzolanic activity. Specifically, the Si–O–Si and Al–O–Si stretching vibrations observed in the 1000-1100 cm^{-1} range indicate the retention of primary aluminosilicate units, which are vital for pozzolanic reactivity. The presence of these bonds suggests that thermally treated montmorillonite maintains its aluminosilicate structure, allowing for effective interaction with calcium hydroxide during hydration. This reaction forms additional C-S-H and C-A-H phases, which are responsible for the increased strength of the mortar composites.

Table 5. Infrared Spectral (FTIR) Characterization of the Montmorillonite

Wavenumber Range (cm^{-1})	Wavenumber Range (cm^{-1})	Wavenumber Range (cm^{-1})
1000-1100	Si–O–Si stretching vibrations	Indicative of the primary structural units of the aluminosilicate framework
790-910	Al-O-Si, Al-OH bonds	Characteristic peaks of aluminosilicate systems
600-750	Al-O, Fe-O bonds	Evidence of the presence of silicoaluminate phases
3000-3600	Broad –OH absorption	Attributed to residual/hydration water and weakly bound molecular species
4000-3800	Weak OH absorption	Characteristic feature of thermally treated pozzolanic additives
400-420(inset)	Deformation vibrations of metal–oxide bonds	Suggests partial retention or reorganization of structural units

Additionally, the Al-O-Si and Al-OH peaks observed in the 790-910 cm^{-1} range confirm the presence of aluminosilicate phases, which are critical for the pozzolanic reactivity of the material. The metal-oxide bond deformation vibrations (400-420 cm^{-1}) further suggest that ion exchange and structural reorganization occur, which can enhance the binding capacity of the material and improve the overall cohesion of the composite, contributing to better mechanical strength.

The XRD analysis (Table 6) offers valuable insights into the structural behavior of the material under study. The identified phases, which include montmorillonite, illite, and cristobalite, alongside the aluminosilicate network observed at 18.27° (2θ), confirm the existence of a layered silicate structure typical of montmorillonite. The diffraction patterns suggest that montmorillonite retains some structural stability while also demonstrating an ability to undergo structural reorganization and engage in pozzolanic reactions. The transformations mentioned, which likely involve ion exchange and dissolution–precipitation mechanisms, facilitate the formation of stable hydration products, including calcium silicate hydrate (C–S–H) and calcium aluminate hydrate (C–A–H). The formation of these denser and more durable phases enhances the mechanical strength and overall durability of the composite mortar.

Table 6. XRD Analysis of the Mineralogical Components

Phase / Mineral	2θ (°)	d (Å)	Description
Quartz (SiO_2)	26.6	3.34	Main diffraction peak
Montmorillonit	6.0	-	(001) reflection, layered structure
Illite	6–10	-	Layered silicate
Cristobalite	-	-	Secondary phase identified by usage
Aluminosilicate network	18.27	4.853	Indicator of structural transform
Aluminosilicate network	93.19	1.06	Indicator of structural transform

3.2. TG/DTG, TG/DSC, and TG/MS Methods

For a comprehensive assessment of the pozzolanic activity, the thermal behavior of the montmorillonite sample was investigated using TG/DTG, TG/DSC, and TG/MS techniques (Figure 4, Table 7). These complementary methods provide a multi-perspective understanding of the thermal stability, phase transitions, and gas evolution associated with the structural decomposition of montmorillonite

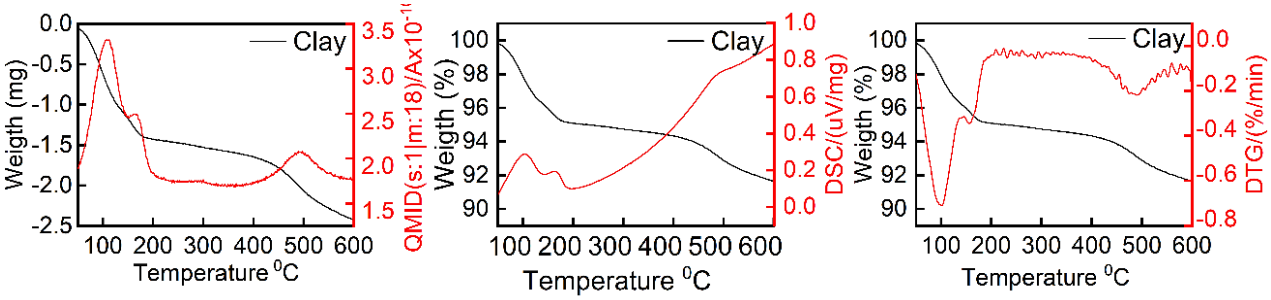

Figure 4. Comprehensive thermal analysis of montmorillonite using TG/DTG, TG/DSC, and TG/MS methods

Table 7. Comparison of TG/DTG, TG/DSC, and TG/MS Methods

Aspect	TG/DTG	TG/DSC	TG/MS
Thermal Events Identified	Free water loss, chemically bound water release, dehydroxylation	Endothermic reactions corresponding to water release and dehydroxylation	Identification of evolved gases (mainly H_2O)
Mass Loss Behavior	Quantified in % mass loss steps	Aligned with TG results	Direct detection and quantification of evolved gases
Peak information (Temp & intensity)	Peaks at 101,1°C, 156,7°C, 490,3°C; max rate -0.71%/min	Peaks at 102,3°C, 161,7°C, 485,5°C; heat flow peaks quantified	Peaks at 104,7°C, 162,9°C, 489,5°C; ion current
Main Analytical Contribution	Precise phase transition timing and mass loss rate	Determination of thermal energy involved in transformations	Identification of evolved gases (mainly H_2O)
Evolved Gases Detection	No direct gas detection	No direct gas detection	Direct detection and quantification of evolved gases
Overall Applicability	Quantitative analysis of thermal stability and reaction stages	Thermodynamic insight and energy requirements for phase changes	Complementary to TG/DTG & TG/DSC by providing chemical specificity

Thermal analysis revealed a sequence of mass loss events corresponding to the release of physically adsorbed water, dehydroxylation of structural hydroxyl groups, and evolution of carbon dioxide. Specifically, the initial endothermic peaks observed at approximately 100–160 °C in both the TG/DTG and TG/DSC profiles were attributed to the desorption of free and interlayer water molecules. This process reflects the weakly bound nature of the surface and interlamellar water, which is a characteristic feature of layered silicate structures. The subsequent major endothermic event between approximately 450 and 500 °C corresponds to the dehydroxylation of the octahedral layers, as confirmed by the TG/MS detection of water vapor evolution. This step signifies a significant structural transformation, marking the disruption of the montmorillonite lattice and the release of reactive aluminosilicate species.

The detection of CO_2 evolution at higher temperatures further suggests the presence of minor carbonate impurities or secondary reactions involving surface-bound carbonates in the sample. The progressive mass loss and associated endothermic reactions provide evidence of the thermal activation potential of the sample. Dehydroxylation, in particular, produces an amorphous aluminosilicate phase that exhibits enhanced pozzolanic reactivity because the loss of hydroxyl groups creates active sites capable of reacting with calcium hydroxide during hydration.

Collectively, the combined TG/DTG, TG/DSC, and TG/MS analyses confirmed that montmorillonite undergoes a series of well-defined thermal transformations that release volatile components (H_2O and CO_2) and lead to the formation of reactive metastable phases. These processes underpin its ability to contribute to the generation of hydration products, such as calcium silicate hydrate (C–S–H) and calcium aluminate hydrate (C–A–H), thereby reinforcing its suitability as a pozzolanic additive in cementitious systems.

3.3. The Rheological and Physical Properties of Composite Mortar Mixes

The rheological and physical properties of the composite mortars are listed in Table 8. The fresh and hardened densities indicated that the addition of montmorillonite and basalt fibers affected the packing and compactness of the mortar matrix. Specifically, increasing the montmorillonite content from 5% to 25% led to higher fresh and hardened densities, reflecting enhanced particle packing and filler effects.

Table 8. Rheological and Physical Properties of Composite Mortar Mixes

Material	Fresh Mortar Density (kg/m³)	Hardened Mortar Density (kg/m³)	Flow (cm)
Control	1860	1645	18
CM 5%	1789	1632	17.5
CM 15%	1929	1768	17
CM 25%	1952	1889	12
CM 15% +F 0.5%	1779	1.666	17
CM 15% +F 1%	2077	1858	16
CM 15% +F 2%	2018	1799	13

The incorporation of basalt fibers also influenced the density and flow behavior. While the addition of 0.5–1% fiber slightly increased the fresh and hardened densities, the 2% fiber content produced a denser matrix but reduced workability, as evidenced by the decrease in flow from 18 cm (control) to 13 cm. Overall, the results demonstrate a trade-off between matrix densification and workability: montmorillonite and fiber addition improve density and structural integrity but can reduce the fresh mortar flow at higher contents, consistent with standard rheological expectations (ASTM C230) [48].

For each component, the final value of the flexural strength was determined by calculating the mean of three identical test samples, while the compressive strength was derived from the average of six halves obtained from the flexural test. The results are presented in Table 9 and Figure 5.

Table 9. Compositions of cement mortars and averaged data of the main physical and mechanical characteristics

N	Material	Water absorption, (%)		Flexural strength, (MPa)		Compressive strength, (MPa)	
		7 days	28 days	7 days	28 days	7 days	28 days
1	Control	12.25	9.16	0.696	1.143	4.318	7.464
2	CM 15%	12.8	7.9	1.757	2.134	7.145	10.482
3	CM 15% +F 0.5%	11.35	7.83	0.994	1.051	5.45	7.892
4	CM 15% +F 1%	8.58	7.38	3.341	3.255	13.309	16.555
5	CM 15% +F 2%	12.92	7.33	2.812	4.331	12.086	18.359

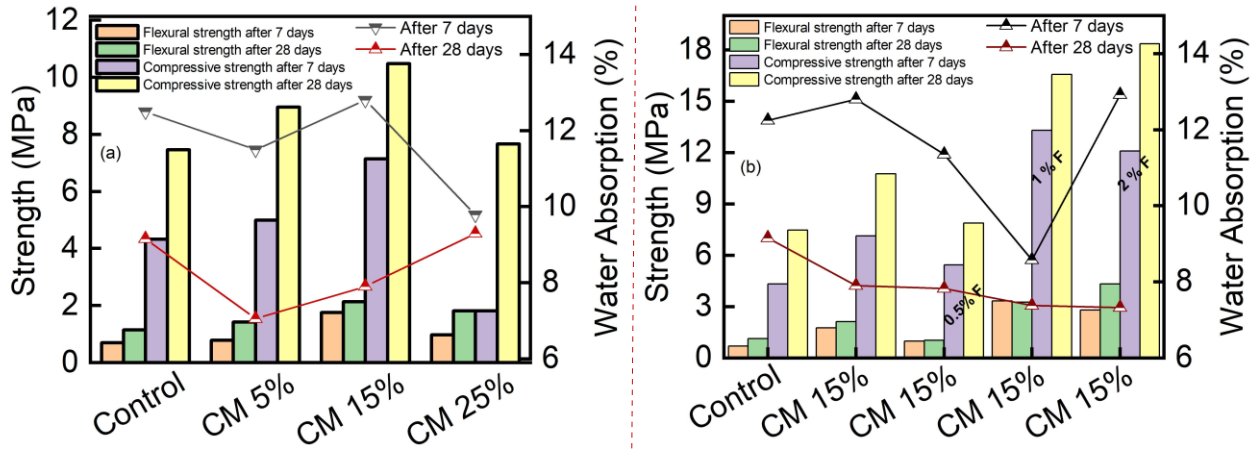

Figure 5. Comparison of (a) mechanical and (b) hydraulic properties of complex mortars based on clay and clay/basalt microfiber composites

Based on the results presented in Table 9 and Figure 5, the mixture containing 1% basalt fibers (CM 15% + F 1%) demonstrated excellent early age performance, characterized by the lowest early stage water absorption. However, the mixture with 2% basalt fibers (CM 15% + F 2%) exhibited superior long-term mechanical properties. Specifically, it achieved the highest compressive (18.36 MPa) and flexural (4.33 MPa) strengths at 28 d, suggesting enhanced fiber-matrix interactions, improved hydration product formation, and superior crack-bridging capabilities. Although the 7-day flexural strength of the 2% basalt fiber mix was slightly lower than that of the 1% fiber mix, the overall long-term performance, matrix densification, and durability of the 2% fiber-reinforced system render it the optimal composition for the montmorillonite-based composite mortar developed in this study.

The inclusion of 2% basalt fibers in the 15% montmorillonite mixture resulted in substantial improvements in the long-term mechanical performance. Compared to the control mix, the compressive strength increased by approximately 180% at 7 days and 146% at 28 days, whereas the flexural strength increased by 304% at 7 days and 279% at 28 days. In terms of durability, the 28-day water absorption of the CM 15% + F 2% mix decreased by approximately 20% relative to that of the control mix, indicating effective densification of the matrix and enhanced resistance to moisture ingress. Although the 7-day water absorption slightly increased owing to the early stage addition of fibers, the overall long-term reduction demonstrates the improved performance and durability of the optimized composite mortar system.

3.3.1. Correlation with Mechanical Strength

The mechanical strength trends observed in the mortar composites, particularly the maximum strength achieved with 15% montmorillonite additive (Figure 5 and Table 9), can be directly attributed to these structural and chemical transformations. The formation of secondary C-S-H and C-A-H phases, as indicated by both FTIR and XRD, contributed to the densification of the material, improving its binding capacity and reducing its porosity. This resulted in increased compressive strength and reduced water absorption, which are key indicators of mortar performance. Furthermore, the amorphous nature of montmorillonite and its fine particle size, as suggested by the FTIR and XRD findings, enhanced the ability of the material to act as a microfiller, improving the overall homogeneity and physical properties of the composite. The higher surface area and potential for more effective pozzolanic reactions further support the enhanced strength and durability of the mortars.

In conclusion, the FTIR and XRD results provide significant evidence that the montmorillonite additive undergoes structural changes during hydration, leading to the formation of hydration products that improve the mechanical properties of the composite mortars. These findings directly correlate with the observed mechanical strength trends and support the high pozzolanic reactivity and durability of this material.

3.4. BET Analysis

The high specific surface area, mesoporous structure, and uniform particle distribution of montmorillonite play crucial roles in promoting hydration and pozzolanic reactions by providing extensive reactive interfaces and facilitating ion diffusion. BET and DLS analyses (Figure 6 and Table 10) confirmed these features, showing Type IV nitrogen adsorption–desorption isotherms with H_3 hysteresis loops, which are characteristic of mesoporous materials. Upon the incorporation of basalt fibers, the isotherms displayed a reduced total adsorption volume and a narrower hysteresis loop, indicating partial pore filling and decreased mesoporous connectivity. Correspondingly, the BJH pore size distribution shifted toward smaller diameters (from 3–7 nm to 2.2–4 nm), reflecting the pore refinement and structural densification of the composite. This decrease in surface area and pore volume is associated with the progressive occupation of mesopores by hydration products, such as C–S–H and C–A–H, leading to a more compact microstructure. These textural modifications enhance the mechanical performance and durability of the composite mortar by reducing permeability and promoting efficient pozzolanic reactions.

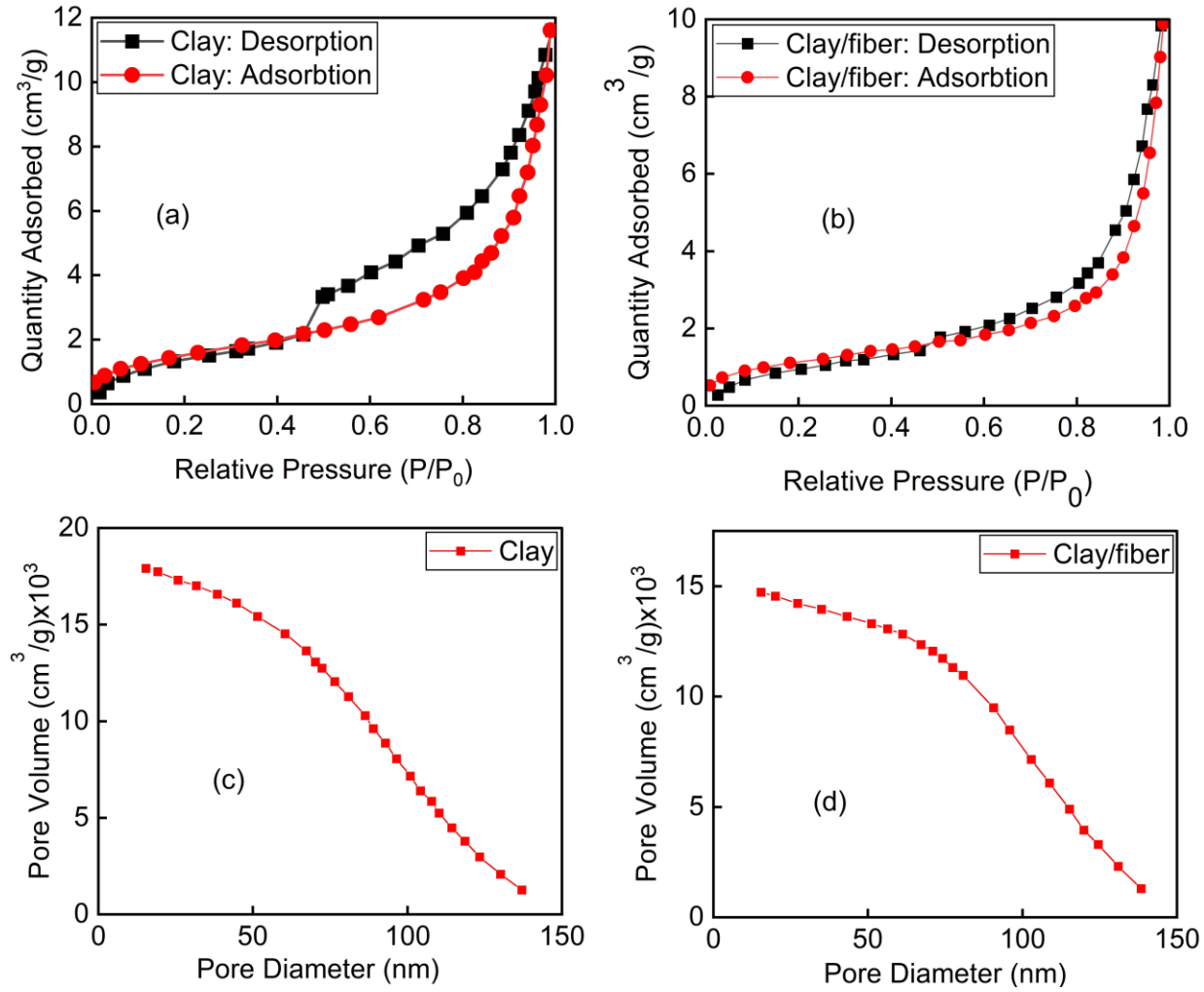

Figure 6. Nitrogen isotherms and BJH pore size analysis of clay and clay/fiber systems

Table 10. Comparative of Adsorption–Desorption Analysis Results

Property	Montmorillonite Sample	System Reinforced with Basalt Fiber	Change
Isotherm Type	Type IV with hysteresis ($P/P_0 \approx 0.4$–0.9)	Similar Type IV with hysteresis; structural changes observed	–
Total Adsorption (cm^3/g STP)	11.5	~16–17% decrease	Approximately 9.5–9.7 cm^3/g
BET Specific Surface Area (m^2/g)	≈47.78	≈28.5% decrease	≈34.2 m^2/g
Density Modulus (m^2/g)	5.66 ± 0.014	Not specified	-
Average Pore Diameter (nm)	5.77	2.2–4 (by BJH analysis)	Pore narrowing toward micro- to mesoporous range
BJH Dominant Pore Distribution (nm)	3–7	2.2–4	Shift in pore size distribution toward smaller diameters
Total Pore Volume (cm^3/g)	≈0.01795	≈17.9% decrease	≈0.0147 sm^3/g

3.5. SEM Analysis

The incorporation of uniformly distributed basalt microfibers enhanced the mechanical resistance and structural integrity of the composite mortar. SEM observations of samples with 0.5%, 1%, and 2% fiber content (Figure 7) show that the fiber concentration significantly affects the fiber–matrix interface. At 0.5% fiber content, incomplete dispersion and limited bonding created localized porosity and weak interfacial zones. In contrast, the sample with 1% basalt fibers exhibited a dense interfacial transition zone (ITZ) with hydration products uniformly coating the fibers, resulting in effective stress transfer and improved crack resistance. At a higher fiber content (2%), fiber agglomeration and incomplete wetting led to structural discontinuities that weakened matrix cohesion. These microstructural findings correlate with the mechanical behavior shown in Figure 5-b. Consistent with the literature [31, 49, 50], the accumulation of hydration products on the fiber surfaces enhanced fiber–matrix bonding, supporting the improved mechanical cohesion and durability of the optimized composite system.

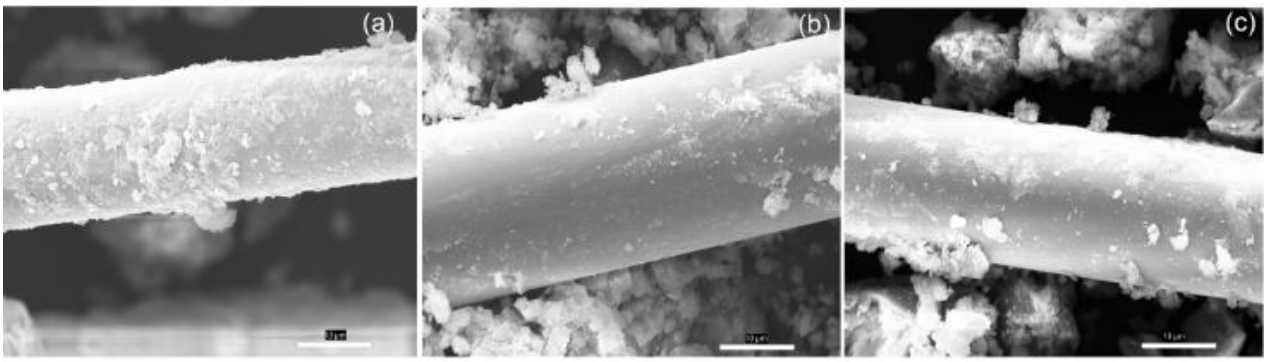

Figure 7. Microstructural interface of basalt microfibers within the mortar matrix at different fiber contents: (a) 0.5% fibers, (b) 1% fibers, and (c) 2% fibers

4. Conclusions

This study investigated the combined incorporation of thermally treated montmorillonite (600 °C), quicklime, and basalt microfibers into cement mortars to enhance their physicomechanical and microstructural performance. The main findings are as follows:

- Thermally treated montmorillonite (15 wt. %) complied with ASTM C618 requirements for Class N pozzolans. Characterization by FTIR, XRD, DLS, and BET confirmed its monodisperse particle size distribution, high specific surface area, mesoporous structure, and partial retention of the aluminosilicate units. These properties promote pozzolanic activity, facilitating the formation of secondary hydration products such as C–S–H and C–A–H.
- The addition of quicklime effectively accelerated the pozzolanic reactions of montmorillonite, enhancing the early age strength. The combined effect of montmorillonite and quicklime produced a denser and more cohesive binder matrix, as confirmed by SEM and BET analyses.
- Composite mortars containing 15 wt.% montmorillonite, 2 wt.% basalt microfibers, and quicklime exhibited the highest mechanical performance, achieving compressive and flexural strengths of 18.36 MPa and 4.33 MPa, respectively, at 28 days. The 1 wt% fiber mix demonstrated excellent early-age performance (7-day compressive strength 16.56 MPa, flexural strength 3.26 MPa) and the lowest early water absorption (8.58%).
- Water absorption decreased by nearly 20% compared to that of the control mix, demonstrating improved compactness, reduced permeability, and enhanced resistance to moisture ingress.
- Overall, the synergistic incorporation of thermally treated montmorillonite, quicklime, and basalt microfibers provides a sustainable strategy for producing high-performance, durable, and eco-efficient mortars suitable for construction applications.
- Future studies should focus on the long-term durability, shrinkage, freeze–thaw resistance, carbonation, and optimization of quicklime content to maximize pozzolanic reactivity and performance in large-scale applications.

5. Declarations

5.1. Author Contributions

Conceptualization, H.K. and M.B.; methodology, H.K., R.S., A.S., and A.B.; software, Y.M.; validation, H.K., M.A., and M.B.; formal analysis, A.A.; investigation, H.K., M.A., R.S., and G.T.; resources, A.S., A.B., G.T., Z.P., and Y.M.; data curation, H.K., Z.P., A.A., and Y.M.; writing—original draft preparation, H.K., M.A., and R.S.; writing—review and editing, H.K., M.A., and R.S.; visualization, H.K., M.A., and R.S.; supervision, M.B.; project administration, M.B. All authors have read and agreed to the published version of the manuscript.

5.2. Data Availability Statement

The data presented in this study are available on request from the corresponding author.

5.3. Funding

The authors received no financial support for the research, authorship, and/or publication of this article.

5.4. Conflicts of Interest

The authors declare no conflict of interest.

6. References

[1] Habert, G., Miller, S. A., John, V. M., Provis, J. L., Favier, A., Horvath, A., & Scrivener, K. L. (2020). Environmental impacts and decarbonization strategies in the cement and concrete industries. Nature Reviews Earth and Environment, 1(11), 559–573. doi:10.1038/s43017-020-0093-3.

[2] Miller, S. A., & Moore, F. C. (2020). Climate and health damages from global concrete production. Nature Climate Change, 10(5), 439–443. doi:10.1038/s41558-020-0733-0.

[3] Capros, P., Kouvaritakis, N., Mantzos, L., & Hendriks, C. (2001). Economic evaluation of sectoral emission reduction objectives for climate change. Top-down analysis of greenhouse gas emission reduction possibilities in the EU. Final Report, TRN: GR04CC101, National Technical University of Athens NTUA, Athens, Greece.

[4] Scrivener, K. L., John, V. M., & Gartner, E. M. (2018). Eco-efficient cements: Potential economically viable solutions for a low-CO2 cement-based materials industry. Cement and Concrete Research, 114, 2–26. doi:10.1016/j.cemconres.2018.03.015.

[5] Amran, M., Makul, N., Fediuk, R., Lee, Y. H., Vatin, N. I., Lee, Y. Y., & Mohammed, K. (2022). Global carbon recoverability experiences from the cement industry. Case Studies in Construction Materials, 17, 1439. doi:10.1016/j.cscm.2022.e01439.

[6] Hussein, A. O., Ghayyib, R. J., Radi, F. M., Jawad, Z. F., Nasr, M. S., & Shubbar, A. (2024). Recycling of Eggshell Powder and Wheat Straw Ash as Cement Replacement Materials in Mortar. Civil Engineering Journal, 10(1), 83–99. doi:10.28991/CEJ-2024-010-01-05.

[7] Andrew, R. M. (2019). Global CO2 emissions from cement production, 1928-2018. Earth System Science Data, 11(4), 1675–1710. doi:10.5194/essd-11-1675-2019.

[8] Cristelo, N., Segadães, L., Coelho, J., Chaves, B., Sousa, N. R., & de Lurdes Lopes, M. (2020). Recycling municipal solid waste incineration slag and fly ash as precursors in low-range alkaline cements. Waste Management, 104, 60–73. doi:10.1016/j.wasman.2020.01.013.

[9] Gartner, E., & Sui, T. (2018). Alternative cement clinkers. Cement and Concrete Research, 114, 27–39. doi:10.1016/j.cemconres.2017.02.002.

[10] Li, C., Gong, X., Cui, S., Wang, Z., Zheng, Y., & Chi, B. (2011). CO2 emissions due to cement manufacture. Materials Science Forum, 685, 181–187. doi:10.4028/www.scientific.net/MSF.685.181.

[11] Maji, I. K., & Adamu, S. (2021). The impact of renewable energy consumption on sectoral environmental quality in Nigeria. Cleaner Environmental Systems, 2, 100009. doi:10.1016/j.cesys.2021.100009.

[12] Peng, J., Huang, L., Zhao, Y., Chen, P., Zeng, L., & Zheng, W. (2013). Modeling of carbon dioxide measurement on cement plants. Advanced Materials Research, 610–613, 2120–2128. doi:10.4028/www.scientific.net/AMR.610-613.2120.

[13] Cheng, D., Reiner, D. M., Yang, F., Cui, C., Meng, J., Shan, Y., Liu, Y., Tao, S., & Guan, D. (2023). Projecting future carbon emissions from cement production in developing countries. Nature Communications, 14(1), 8213. doi:10.1038/s41467-023-43660-x.

[14] Khaiyum, M. Z., Sarker, S., & Kabir, G. (2023). Evaluation of Carbon Emission Factors in the Cement Industry: An Emerging Economy Context. Sustainability (Switzerland), 15(21), 15407. doi:10.3390/su152115407.

[15] Ragab, A. E.-R., Younis, S., & Mohamed Moawad, M. S. (2022). Green Building: Use of Pozzolanic Material to Reduce CO_2 Emissions and Energy Conservation in the Production of Composite Pozzolanic Cement. American Journal of Engineering and Applied Sciences, 15(2), 132–139. doi:10.3844/ajeassp.2022.132.139.

[16] Marandi, N., & Shirzad, S. (2025). Sustainable cement and concrete technologies: a review of materials and processes for carbon reduction. Innovative Infrastructure Solutions, 10(9), 408. doi:10.1007/s41062-025-02213-5.

[17] Flower, D. J. M., & Sanjayan, J. G. (2007). Greenhouse gas emissions due to concrete manufacture. International Journal of Life Cycle Assessment, 12(5), 282–288. doi:10.1065/lca2007.05.327.

[18] Jhatial, A. A., Nováková, I., & Gjerløw, E. (2023). A Review on Emerging Cementitious Materials, Reactivity Evaluation and Treatment Methods. Buildings, 13(2), 526. doi:10.3390/buildings13020526.

[19] Mohsen, M. O., Aburumman, M. O., Al Diseet, M. M., Taha, R., Abdel-Jaber, M., Senouci, A., & Abu Taqa, A. (2023). Fly Ash and Natural Pozzolana Impacts on Sustainable Concrete Permeability and Mechanical Properties. Buildings, 13(8), 1927. doi:10.3390/buildings13081927.

[20] Abed Shnait, M., & Izzet, A. F. (2024). Flexural Behavior of Reinforced Concrete Beams with Steel-Plate Reinforced Vertical Opening. Civil Engineering Journal, 10(9), 2820–2838. doi:10.28991/CEJ-2024-010-09-04.

[21] Etxebarria, I., Veneranda, M., Costantini, I., Prieto-Taboada, N., Larrañaga, A., Marieta, C., De Nigris, B., Martellone, A., Amoretti, V., Arana, G., Madariaga, J. M., & Castro, K. (2023). Testing the volcanic material burying Pompeii as pozzolanic component for compatible conservation mortars. Case Studies in Construction Materials, 18, 2194. doi:10.1016/j.cscm.2023.e02194.

[22] Marra, F., Danti, A., & Gaeta, M. (2015). The volcanic aggregate of ancient Roman mortars from the Capitoline Hill: Petrographic criteria for identification of Rome's "pozzolans" and historical implications. Journal of Volcanology and Geothermal Research, 308, 113–126. doi:10.1016/j.jvolgeores.2015.10.007.

[23] Seymour, L. M., Maragh, J., Sabatini, P., Tommaso, M. Di, Weaver, J. C., & Masic, A. (2023). Hot mixing: Mechanistic insights into the durability of ancient Roman concrete. Science Advances, 9(1), 1602. doi:10.1126/sciadv.add1602.

[24] Karamyan, H., Sahakov, A., Aperyan, A., Badalyan, M., & Baghdagyulyan, A. (2023). Analyses of the Structure Formation of Constructional Complex Mixtures Developed on a Local Raw Basis and Their Behaviour in a Chemically Aggressive Environment. Key Engineering Materials, 958, 201–207. doi:10.4028/p-hNy5Or.

[25] Qaramyan, H. (2022). Development of dry sand-lime new multicomponent mortars into the historical cultural monuments applied on local raw basis. Key Engineering Materials, 906 KEM, 53–58. doi:10.4028/www.scientific.net/KEM.906.53.

[26] Amsalu Fode, T., Chande Jande, Y. A., & Kivevele, T. (2024). Modeling and Optimization of Sisal Fiber Degradation Treatment by Calcined Bentonite for Cement Composite Materials. Journal of Natural Fibers, 21(1), 2408632. doi:10.1080/15440478.2024.2408632.

[27] Mehta, P.K. and Monteiro, P.J.M. (2006) Concrete: Microstructure, Properties, and Materials (3rd Ed.). McGraw-Hill, New York, United States.

[28] Shao, W., Cao, R., Zhang, W., & Shi, D. (2025). Experimental study on the compressive mechanical behavior and constitutive model of basalt fiber reinforced coral concrete. Construction and Building Materials, 489, 142284. doi:10.1016/j.conbuildmat.2025.142284.

[29] Zheng, H., Zhang, W., Li, B., Zhu, J., Wang, C., Song, G., Wu, G., Yang, X., Huang, Y., & Ma, L. (2022). Recent advances of interphases in carbon fiber-reinforced polymer composites: A review. Composites Part B: Engineering, 233, 109639. doi:10.1016/j.compositesb.2022.109639.

[30] Zhang, F., Lu, Z., & Wang, D. (2024). Working and mechanical properties of waste glass fiber reinforced self-compacting recycled concrete. Construction and Building Materials, 439, 137172. doi:10.1016/j.conbuildmat.2024.137172.

[31] Khandelwal, S., & Rhee, K. Y. (2020). Recent advances in basalt-fiber-reinforced composites: Tailoring the fiber-matrix interface. Composites Part B: Engineering, 192, 108011. doi:10.1016/j.compositesb.2020.108011.

[32] Branston, J., Das, S., Kenno, S. Y., & Taylor, C. (2016). Mechanical behaviour of basalt fibre reinforced concrete. Construction and Building Materials, 124, 878–886. doi:10.1016/j.conbuildmat.2016.08.009.

[33] Ou, Y., Zhu, D., & Li, H. (2016). Strain Rate and Temperature Effects on the Dynamic Tensile Behaviors of Basalt Fiber Bundles and Reinforced Polymer Composite. Journal of Materials in Civil Engineering, 28(10), 04016101. doi:10.1061/(asce)mt.1943-5533.0001615.

[34] Iorio, M., Santarelli, M. L., González-Gaitano, G., & González-Benito, J. (2018). Surface modification and characterization of basalt fibers as potential reinforcement of concretes. Applied Surface Science, 427(Part A), 1248–1256. doi:10.1016/j.apsusc.2017.08.196.

[35] Yang, W., Liu, H., & Wang, H. (2024). Experimental study on mechanical properties of basalt fiber reinforced nano-SiO_2 concrete after high temperature. Frontiers in Materials, 11, 1415144. doi:10.3389/fmats.2024.1415144.

[36] Zhou, H., Jia, B., Huang, H., & Mou, Y. (2020). Experimental study on basic mechanical properties of basalt fiber reinforced concrete. Materials, 13(6). doi:10.3390/ma13061362.

[37] Karapetyan, A., Badalyan, M., Arzumanyan, A., Muradyan, N., & Grigoryan, A. (2023). Study of Physical and Mechanical Properties of Fiber Concretes with Different Compositions. The 4th International Electronic Conference on Applied Sciences, 224. doi:10.3390/asec2023-15930.

[38] Wang, W., Zhang, Y., Mo, Z., Chouw, N., Jayaraman, K., & Xu, Z. dong. (2023). A critical review on the properties of natural fibre reinforced concrete composites subjected to impact loading. Journal of Building Engineering, 77, 107497. doi:10.1016/j.jobe.2023.107497.

[39] Pinheiro, V. D., Abreu, R. F. de, Alexandre, J., Xavier, G. de C., Marvila, M. T., & de Azevedo, A. R. G. (2024). Pozzolanic Potential of Calcined Clays at Medium Temperature as Supplementary Cementitious Material. Sustainability (Switzerland), 16(17), 7508. doi:10.3390/su16177508.

[40] Balykov, A. S., Nizina, T. A., Volodin, V. V., & Kyashkin, V. M. (2021). Effects of Calcination Temperature and Time on the Physical-Chemical Efficiency of Thermally Activated Clays in Cement Systems. Materials Science Forum, 1017, 61–70. doi:10.4028/www.scientific.net/msf.1017.61.

[41] Akbulut, Z. F., Kuzielová, E., Tawfik, T. A., Smarzewski, P., & Guler, S. (2024). Synergistic Effects of Polypropylene Fibers and Silica Fume on Structural Lightweight Concrete: Analysis of Workability, Thermal Conductivity, and Strength Properties. Materials, 17(20), 5042. doi:10.3390/ma17205042.

[42] Gu, L., Liu, Y., Zeng, J., Zhang, Z., Pham, P. N., Liu, C., & Zhuge, Y. (2024). The synergistic effects of fibres on mechanical properties of recycled aggregate concrete: A comprehensive review. Construction and Building Materials, 436, 137011. doi:10.1016/j.conbuildmat.2024.137011.

[43] Shainova, R. S., Karamyan, H. H., Sahakyan, A. T., Avagyan, M. A., & Aperyan, A. J. (2024). Development of complex mortars based on bentonite clay. XIII International Conference on Chemistry for Young Scientists, 2-6 September, 2024, St Petersburg, Russia.

[44] ASTM C618-17a. (2019). Standard Specification for Coal Fly Ash and Raw or Calcined Natural Pozzolan for Use in Concrete. ASTM International, Pennsylvania, United States. doi:10.1520/C0618-17A.

[45] GOST 31108-2020. (2019). Cements for General Construction. Technical Conditions. Publishing House Standard, Moscow, Russia.

[46] EN 196-1-2002. (2002). Methods of testing cement. Part 1. Determination of strength. European Committee for Standardization, Brussels, Belgium.

[47] EN 196-2-2002. (2002). Methods of testing cement - Part 2: Chemical analysis of cement. European Committee for Standardization, Brussels, Belgium.

[48] ASTM C230/C230M-98E1. (2013). Standard Specification for Flow Table for Use in Tests of Hydraulic Cement. ASTM International, Pennsylvania, United States. doi:10.1520/C0230_C0230M-98E01.

[49] Castro-Cabrera, I., Chénier, A., Blanchard, A., Gérard, J. F., Lortie, F., & Rumeau-Duchet, J. (2025). Methodical approach to interface design: Role of sizing in the micro-mechanical performance and durability of basalt fibers-based composites. Materialia, 42, 102467. doi:10.1016/j.mtla.2025.102467.

[50] Qin, X., Shen, A., & Guo, Y. (2016). Experimental study on road performance of basalt fiber reinforced bitumen mastics. Jianzhu Cailiao Xuebao/Journal of Building Materials, 19(4), 659–664. doi:10.3969/j.issn.1007-9629.2016.04.009.